Direct Observation of Nitrogen Location in Molecular Beam Epitaxy Grown Nitrogen-Doped ZnO

Paul Fons,* Hiroshi Tampo, Alexander V. Kolobov, Masataka Ohkubo, Shigeru Niki, and Junji Tominaga
National Institute of Advanced Industrial Science & Technology, Tsukuba Central 4, Higashi 1-1-1, Tsukuba, Ibaraki, 305-8562, Japan

Roberta Carboni and Federico Boscherini
Department of Physics and CNISM, University of Bologna, viale C. Berti Pichat 6/2, 40127 Bologna, Italy

Stephan Friedrich
Advanced Detector Group, L-270 Lawrence Livermore National Laboratory, Livermore, California 94550, USA
(Received 27 October 2005; published 2 February 2006)

ZnO is a wide band gap, naturally *n*-type semiconductor with great promise for optoelectronic applications; the main obstacle yet to be overcome is *p*-type doping. Nitrogen, the most promising candidate currently being pursued as a dopant, has been predicted to preferentially incorporate into the ZnO lattice in the form of a N_2^- molecule at an O site when a plasma source is used, leading to compensation rather than *p*-type doping. We demonstrate this to be incorrect by using N *K*-edge x-ray absorption spectra and comparing them with first-principles calculations showing that nitrogen, in fact, incorporates substitutionally at O sites where it is expected to act as an acceptor. We also detect the formation of molecular nitrogen upon annealing. These results suggest that effective *p*-type doping of ZnO with N may be possible only for low-temperature growth processes.

DOI: 10.1103/PhysRevLett.96.045504 PACS numbers: 68.55.Ln, 61.10.Ht, 66.30.Jt, 71.15.Mb

The wide band-gap semiconductor ZnO has recently attracted renewed interest as a possible optoelectronic material. ZnO is in many ways similar to GaN, but has several strong advantages. It has a near-UV band gap, and bulk substrates are available. ZnO is inexpensive, mechanically hard, and optically active even with high dislocation densities. The high stability (60 meV), large oscillator strength, and narrow optical gain energy distribution of excitons in ZnO suggest that significant improvements over free carrier recombination devices can be achieved opening the door to a new generation of excitonic devices. The only major drawback to the wide-scale use of ZnO for device applications is the difficulty to dope it *p* type. Although there have been reports of *p*-type doping in the literature, they have been plagued by lack of reproducibility, strongly suggesting the physics of the doping process is subtle.

Nitrogen is widely considered to be the most promising *p*-type dopant due to its similar size to oxygen, its resistance to forming *AX* centers [1], and its successful use in other II-VI compounds such as ZnSe [2]. To date, however, experiments attempting to grow *p*-type material have been unsuccessful or difficult to reproduce. Experimentally, several issues complicate a straightforward conclusion regarding the efficacy of N doping. ZnO is a well known transparent conducting oxide due to the low activation energy of donors both from impurities and point defects [3]. In contrast to studies of N doping in other large band-gap II-VI compounds such as ZnSe [2], N acceptors in ZnO are anticipated to have a large activation energy. Theory also predicts that hydrogen induces shallow donor states in ZnO [4], implying that unintentional incorporation of H during growth may result in compensated material; experiment has confirmed this [5,6]. There are also indications that the thermodynamics of N incorporation is complicated. Recent work using a focused laser to rapidly heat and cool a substrate during growth to activate N doping underscore the need for a more comprehensive, fundamental understanding of the physics of N incorporation [7]. Because of the ambiguity of the experimental data in the literature, deeper insight into the energetics of N incorporation in ZnO would offer a useful additional perspective. Recently, first-principles calculations based upon density functional theory (DFT) have been applied to determine the formation energy of various types of compensating defects for nitrogen-doped ZnO in the presence of a plasma source [8,9]. By using a value for the N chemical potential that took into account the presence of a mixture of ground and excited state N_2 in the doping flux, it was shown that the calculated N maximum solubility increased over 8 orders of magnitude with the use of a plasma N source. Concomitant with the use of a plasma N source, it was also found that the dominant N-related defect (with the lowest formation energy) was the formation of an N_2 defect at an O site. The conclusion drawn was that self-compensation effects would always lead to electron dominated conduction. Since these calculations rely on small differences between large numbers, confirmation by experiment is desirable.

Although epitaxial ZnO has been grown by a variety of techniques including rf sputtering [10], MO-chemical va-

por deposition [11], and laser ablation [12] among others, we focus here on radical source–molecular beam epitaxy (RS-MBE) [13]. In RS-MBE, Zn flux is provided by an elemental (7N) effusion cell while O and N fluxes originate from rf-radical cells [14]. The RS-MBE plasma N_2^* source is a near-ideal experimental analog to the calculations referenced above. ZnO samples were grown on both $\{11\bar{2}0\}$ sapphire substrates and the (0001) face of ZnO single-crystal substrates using RS-MBE [15]. The film growth temperature was fixed at 450 °C for all samples; sample thickness was approximately 1000 nm. While the polarity of ZnO epilayers is $(000\bar{1})$ (O face) for growth on conventional sapphire substrates [16], use of the Zn face (0001) of bulk ZnO substrates was found to lead to approximately an order of magnitude increase in N incorporation for otherwise identical growth conditions as measured by calibrated secondary ion mass-spectroscopy (SIMS); this variation arises from differences in surface kinetics due to the change in dangling bond density with inversion. Samples with a variety of N_2 flow rates with differing Zn-O ratios were grown. In this Letter, we focus upon samples grown on the (0001) face of ZnO single crystals due to the larger N concentrations. For the as-grown samples, calibrated SIMS depth profiling measurements indicated a nearly constant N signal with average N concentrations approaching 1% ($[\mathrm{N}] \sim 3 \times 10^{20}$ cm^{-3}). After growth, all samples were divided into two pieces: one half was retained as an as-grown standard, while the other half underwent rapid thermal annealing (RTA) to investigate thermal stability. While as-grown samples were yellow in color, the RTA samples after heating to 800 °C for 3 min became perfectly transparent. SIMS measurements of post-RTA samples revealed almost no change in $[\mathrm{N}]$ ($\sim 2 \times 10^{20}$ cm^{-3}). Electrical measurements using the Hall effect with a van der Pauw geometry were carried out on both as-grown and annealed ZnO:N samples. As the carrier density of the hydrothermally grown ZnO substrates was $n < 10^{12}$ cm^{-3}, the electrical measurements reflect the characteristics of the epilayer alone. For the sample referred to above, the initial electron carrier concentration was found to be 5.6×10^{15} cm^{-3} ($\mu = 12$ cm^2/V s), rising to 6.2×10^{17} cm^{-3} ($\mu = 72$ cm^2/V s) after RTA processing. For reference, the carrier concentration in an undoped ZnO film is typically $\lesssim 1 \times 10^{17}$ cm^{-3}

In order to insightfully choose among growth conditions and to obtain deeper insight into the physics of the doping process, a technique that allows for direct observation of where N incorporates in the ZnO lattice is required. Earlier studies to determine the location of interstitial N in the lattice such as x-ray photoelectron spectroscopy [6] and optically detected magnetic resonance [17] did not reach definitive conclusions due to surface contamination and the inability to unambiguously identify signals arising from N, respectively. In part, because of its elemental selectivity, x-ray absorption fine structure (XAFS) has been long used to provide unique information on the local geometric arrangement of dopants and defects in semiconductors [18]. Indeed, analysis of the extended part of the spectrum (the "EXAFS" region) has been used to determine the dopant coordination in semiconductors. The use of x-ray absorption near-edge structure (XANES) has been limited due to difficulties (real and/or perceived) in simulating the spectra region in which the multiple-scattering expansion of the XAFS cross section does not converge. As XANES is sensitive to the three-dimensional arrangement of atoms in space, there is significantly more detail accessible on the local structure around the impurity or defect being probed. This is to be contrasted with the one-dimensional radial distribution function like data extractable from EXAFS data. The use of XANES data is opening up new ways to examine the local order about defects and impurities in solids [19]. We have used XANES at the K edge of N and first-principles real-space scattering simulations to directly observe the location of N in the ZnO lattice both in as-grown and thermally annealed states. The elemental selective nature of XAFS in conjunction with the sensitivity of spectra in the near-edge region to the three-dimensional arrangement of atoms provide an excellent test for theoretical calculations of N positions in the ZnO lattice and may lead to a more fundamental understanding of the underlying physics.

Samples were measured at beam line ALOISA at the synchrotron ELETTRA in Trieste, Italy. ALOISA is equipped with an undulator-wigger insertion device that generates a flux of about 10^{11} photons/s [20]. All samples were measured at 50° incidence. X-ray fluorescence radiation was detected using a windowless single element Ge solid-state detector (SSD) cooled to 77 K. Photon counting techniques allowed measurement of samples with a N concentration exceeding 5×10^{19} cm^{-3}. The relative orientation of the x-ray beam polarization to the crystallographic axes allows probing of bond anisotropy. To investigate for anisotropic bonding, additional polarization dependent XANES data were taken at the Advanced Light Source synchrotron at Lawrence Berkeley National Laboratory using beam line 4.0.2 [21] with a photon flux of 10^{12} photons/s. The beam was linearly polarized such that for a sample incidence angle of 90°, the polarization was in the plane of the sample. N fluorescence was detected using a nine-element, high-resolution superconducting tunnel junction spectrometer [22]. Data were taken at glancing incidence, at approximately 45°, and at near-normal incidence using a linearly polarized x-ray beam.

Data analysis was carried out in two steps. We used ground-state DFT calculations to relax the ZnO lattice around various N defects and then used these relaxed coordinates as input to a real-space, full multiple-scattering simulation for comparison with experiment. In the first step, an impurity N atom was placed at a high symmetry

position in the ZnO lattice, and the surrounding atoms were relaxed to their ground-state positions using DFT calculated Hellmann-Feynman forces and Broyden minimization [23]. Potentials were calculated self-consistently using a conjugate-gradient algorithm [24]. The norm-conserving pseudopotentials in the Troullier-Martins [25] scheme used for the calculation included the $3d^{10}4s^2$ (Zn), $2s^2 2p^4$ (O), and $2s^2 2p^3$ (N) valence electrons as well as nonlocal core corrections [26]. The generalized gradient approximation (GGA) as expressed by the Perdew-Burke-Ernzerhof exchange formulation was used [27]. Calculations were carried out on 32 atom supercells using a plane wave cutoff energy of 50 Hartree. The final atom positions as expressed by the relaxed supercell where embedded into a DFT relaxed ZnO spherical cluster and used as input to the *ab initio* real-space full multiple-scattering code FEFF8 for the calculation of the simulated x-ray absorption spectra [28]. FEFF8 is a fully relativistic, all-electron Green's function code that utilizes a Barth-Hedin formulation for the exchange-correlation part of the potential and the Hedin-Lundqvist self-energy correction. Potentials were calculated self-consistently using a sphere of 0.8 nm diameter. Although the relaxed lattice parameters calculated using local-density approximation/GGA exchange functionals tend to overestimate bond lengths by $\lesssim 1\%$, this systematic small discrepancy is expected to have only a small effect on the calculated x-ray absorption spectra. Convergence studies of cluster size for FEFF8 demonstrated that convergence was reached for cluster sizes greater than 200 atoms; hence all results presented here are for that size.

Figure 1 shows as-grown experimental (top) and simulated spectra for N in various lattice positions including (b) substitutionally on an O site, (c) as molecular N_2 on an O site, (d) as N in a tetrahedral interstitial, (e) as N in a Zn site, and (f) as N in an octahedral interstitial. The only calculated spectra similar to the experimental data are those for N substituting on an O site. This in part reflects the reduced relaxation and preservation of symmetry for the case of N substituting on an O site as well as the multiple-scattering effects unique to this position; even without inclusion of relaxation effects, only the spectra for which N is substitutional on an O site provide a reasonable match to the observed data. In contrast, there was significant lattice relaxation for N in all other locations. The presence of two nonequivalent low symmetry N atom positions for the case of N_2, leads to a XANES spectrum distinctly different from experiment, demonstrating there is a negligible concentration of N_2 O site defects in as-grown material. The excellent agreement between the experimental and simulated XANES spectra demonstrate that N incorporates substitutionally on an O site in the as-grown state and that *p*-type doping *is* possible and not prevented by spontaneous, self-compensating defect generation.

We now turn to the effects of temperature on N-doped ZnO. Although the annealing temperature (800 °C) used in

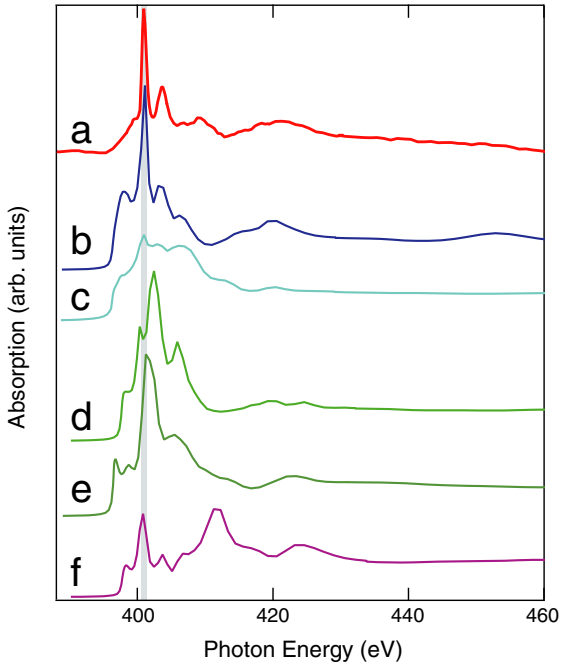

FIG. 1 (color online). Experimental (a) and simulated x-ray absorption spectra for (b) N on an O site, (c) N_2 on an O site, (d) N in a tetrahedral interstitial, (e) N in a Zn site, and (f) N in an octahedral interstitial. The gray band around 400 eV shows the expanded scale of Fig. 2 for reference. The energy step was 0.5 eV.

the current experiment is low compared with the melting point of ZnO (1975 °C) and the annealing time is short (3 min), the XANES spectra changed dramatically upon annealing. High-resolution measurements shown in Fig. 2 clearly demonstrate the presence of an additional structure, namely, the presence of the characteristic features of the nitrogen molecule. Note the use of an expanded energy scale versus Fig. 1. Experimental data for nitrogen gas measured in transmission are also included at the top of the figure for reference. Typical XAFS spectra for a sample that underwent thermal annealing are shown in Fig. 2 as a function of polarization. There is a striking resemblance between the molecular nitrogen gas and the experimental absorption data. In addition, there is no significant change with the polarization implying that the molecular nitrogen is not oriented along a particular crystallographic direction. These facts strongly suggest that the effect of thermal annealing is to induce the formation of N_2 bubbles which have minimal interaction with the ZnO lattice. The inert nature of N in postanneal samples is also manifested by the transformation of the samples from yellow (as-grown) to transparent (postanneal).

We conclude that for RS-MBE epilayers grown on (0001) ZnO single-crystal substrates, N incorporates predominately substitutionally at an O site and at concentrations exceeding 10^{20} cm^{-3}; the electrical compensation

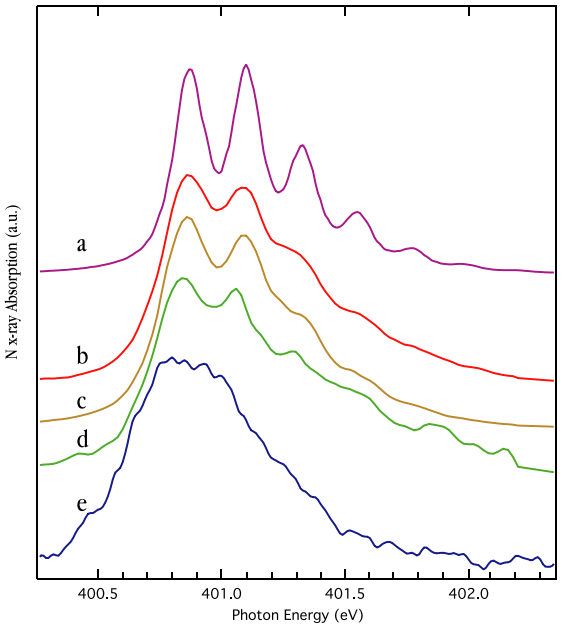

FIG. 2 (color online). N XAFS data for (a) a molecular nitrogen standard and an RTA ZnO:N film with $\vec{E}$ directed along the (b) *c* axis, (c) 45°, in the (d) *ab* plane, and (e) as grown at 45°. The energy step used was 200 meV.

observed is consistent with this conclusion. Although the large chemical concentrations are consistent with the trends that have been predicted for the use of rf-plasma N sources, there is no evidence for the formation of N_2 incorporating on O sites as had been predicted on the basis of formation energy arguments. The metastability of the N incorporation was demonstrated by the rapid movement of N from substitutional O sites to form bubbles, although diffusion arguments would appear to severely limit the size of the bubbles and make direct observation difficult. The above arguments suggest that N incorporation as an acceptor is metastable and that care must be used in interpretation of experimental results.

The DFT results were obtained through the use of the ABINIT code, a common project of the Université Catholique de Louvain, Corning Incorporated, and other contributors (http://www.abinit.org). We are also grateful to the ALOISA staff for help with the experiment. Measurements at ELETTRA were supported by the Synchrotron Radiation Committee of Istituto Nazionale per la Fisica della Materia. S. F. acknowledges NSF, DOE OBER, and NA-22 funding. Part of this work was performed under the auspices of the U.S. Department of Energy by Lawrence Livermore National Laboratory under Contract No. W-7405-ENG-48. We thank Elke Arenholz for providing the gaseous N_2 reference spectrum.

*Electronic addresses: paul-fons@aist.go.jp; http://staff.aist.go.jp/paul-fons

[1] C. H. Park, S. B. Zhang, and S.-H. Wei, Phys. Rev. B **66**, 073202 (2002).
[2] K. Ohkawa, T. Karasawa, and T. Mitsuyu, J. Cryst. Growth **111**, 797 (1991).
[3] D. Look, J. Hemsky, and J. Sizelove, Phys. Rev. Lett. **82**, 2552 (1999).
[4] C. Van de Walle, Phys. Rev. Lett. **85**, 1012 (2000).
[5] E. Lavrov, J. Weber, F. Borrnert, C. V. de Walle, and R. Helbig, Phys. Rev. B **66**, 165205 (2002).
[6] C. Perkins, S. Lee, X. Li, S. Asher, and T. Coutts, J. Appl. Phys. **97**, 034907 (2005).
[7] A. Tsukazaki *et al.*, Nat. Mater. **4**, 42 (2005).
[8] E. Lee, Y. Kim, Y. Jin, and K. Chang, Physica (Amsterdam) **308B**, 912 (2001).
[9] E. Lee, Y. Kim, Y. Jin, and K. Chang, Phys. Rev. B **64**, 085120 (2001).
[10] Y. Igasaki and H. Saito, J. Appl. Phys. **69**, 2190 (1991).
[11] Y. Liu, C. Gorla, S. Liang, N. Emanetoglu, Y. Lu, H. Shen, and M. Wraback, J. Electron. Mater. **29**, 69 (2000).
[12] S. Choopun, R. Vispute, W. Noch, A. Balsamo, R. Sharma, T. Venkatesan, A. Iliadis, and D. Look, Appl. Phys. Lett. **75**, 3947 (1999).
[13] P. Fons, K. Iwata, A. Yamada, K. Matsubara, and S. Niki, J. Cryst. Growth **201–202**, 627 (1999).
[14] P. Fons, K. Iwata, A. Yamada, K. Matsubara, K. Nakahara, T. Tanabe, H. Takasu, and S. Niki, J. Cryst. Growth **227–228**, 911 (2001).
[15] P. Fons, K. Iwata, A. Yamada, K. Matsubara, K. Nakahara, T. Tanabe, H. Takasu, and S. Niki, Appl. Phys. Lett. **77**, 1801 (2000).
[16] T. Ohnishi, A. Ohtomo, M. Kawasaki, K. Takahashi, M. Yoshimoto, and H. Koinuma, Appl. Phys. Lett. **72**, 824 (1998).
[17] G. Aliev, S. Bingham, D. Wolverson, J. Davies, H. Makino, H. Ko, and T. Yao, Phys. Rev. B **70**, 115206 (2004).
[18] J. Knights, T. Hayes, and J. Mikkelsen, Jr., Phys. Rev. Lett. **39**, 712 (1977).
[19] G. Ciatto, F. Boscherini, A. A. Bonapasta, F. Filippone, A. Polimeni, and M. Capizzi, Phys. Rev. B **71**, 201301(R) (2005).
[20] L. Floreano *et al.*, Rev. Sci. Instrum. **70**, 3855 (1999).
[21] A. Young *et al.*, Nucl. Instrum. Methods Phys. Res., Sect. A **467–468**, 549 (2001).
[22] S. Friedrich, T. Funk, O. Drury, S. Labov, and S. Cramer, Rev. Sci. Instrum. **73**, 1629 (2002).
[23] D. Johnson, Phys. Rev. B **38**, 12 807 (1988).
[24] X. Gonze, Phys. Rev. B **54**, 4383 (1996).
[25] N. Troullier and J. L. Martins, Phys. Rev. B **43**, 1993 (1991).
[26] M. Fuchs and M. Scheffler, Comput. Phys. Commun. **119**, 67 (1999).
[27] J. Perdew, K. Burke, and M. Ernzerhof, Phys. Rev. Lett. **77**, 3865 (1996).
[28] A. Ankudinov and J. Rehr, Phys. Rev. B **62**, 2437 (2000).